DOI:10.13476/j.cnki.nsbdqk.2020.0017
吕蕊蕊,郑源,张德虎,等.基于 FBM 模型的轴流泵空化流动特性 CFD 分析[J].南水北调与水利科技,2020,18(1):150-165.
LYU R R,ZHENG Y,ZHANG D H,et al. CFD analysis of cavitation flow for axial-flow pump based on FBM model[J]. South-to-North Water Transfers and Water Science & Technology,2020,18(1):150-165. (in Chinese)

基于 FBM 模型的轴流泵空化流动特性 CFD 分析

吕蕊蕊,郑源,张德虎,于安

(河海大学 能源与电气学院,南京 211100)

摘要:轴流泵运行工况多变,容易发生空化,会严重影响泵的水力性能。为研究轴流泵空化工况下的流动特性,进行了全流道空化流动数值模拟和压力脉动分析,通过比较实验数据和不同湍流模型的计算结果,验证了 FBM 模型在预测轴流泵外特性和空化性能方面的优越性。研究结果表明:FBM 模型预测非设计条件下的数值误差最小,特别是在具有小流量条件的流场中误差最小,其中平均扬程误差 1.19%,平均效率误差 5.31%;FBM 在预测空泡体积数、含气量上的精度均大于其他三种湍流模型,与实验结果最接近;在 NPSH=5.25 m 空化刚开始阶段,叶片上的压力脉动的主要频率位于 f_n 及其倍频处,叶片吸力面的压力监测点由于受到空泡溃灭影响出现大量低频幅值,导叶出口监测点的压力脉动受到导叶片背面流动状态的影响出现大量低频信息。

关键词:湍流模型;误差;外特性;空化性能;压力脉动

中图分类号:TV136.2 **文献标志码**:A **开放科学(资源服务)标识码(OSID)**:

轴流泵由于流量大、结构简单等优点,被广泛应用于灌溉、给排水以及其他需要输送大流量液体的领域中[1]。机组内的空化是影响水泵稳定运行的重要因素,空化的发生会产生强烈的水击,并造成机组过流部件的腐蚀[2]。所以,对水泵内部空化流动特性的研究具有重要意义。张德胜,候敬生等[3-5]通过 SST k-w 湍流模型,对轴流泵进行全流道空化数值模拟;周大庆,冯卫民,王凡,施卫东,宋希杰等[6-10]基于 SST k-w 和 RNG k-ε 分析了导叶角度、入口均匀流、进水旋涡对轴流泵压力脉动特性的影响;蒋文青等[11]分别基于 RNG k-ε 和 SST k-w 模拟了绕水翼、轴流泵的空化流动过程;周颖等[12]通过标准 k-ε 分析了不同空化条件下轴流泵反向发电压力脉动特性;施卫东,陶迎等[13-14]基于 RNG k-ε 湍流模型分析了叶片数、导叶数和叶片角度对轴流泵空化性能的影响;MOSTAFA N H,HOSONO K,MOLOSHNYI O,WU S Q 等[15-18]大都使用 k-ε 对水泵进行空化数值模拟。

对于轴流泵空化数值模拟,湍流模型的选取在一定程度上会影响水泵性能预测的结果[19],近年来 PANS 和以 k-ε 模型[20-21]为基准的修正模型被逐渐运用于水泵的数值模拟中,余志毅,时素果等[22-23]研究结果表明:基于 FBM 的空化数值模拟可以捕捉到更多的流动细节,但鲜有学者将 FBM 模型应用于轴流泵空化数值模拟。本文使用湍流模型 FBM 对轴流泵在设计流量下进行空化定常、非定常数值模拟,验证该模型数值计算的准确性,分析了空化刚开始工况下转轮和导叶内部的压力脉动特性。基于 Rayleigh-Plesset 方程均相流的空化模型适用性较强[24],多数学者采用该空化模型,因此对于轴流泵空化数值计算采用基于 ANSYS CFX 的均相流空化模型。

1 物理模型及数值计算方法

1.1 几何模型

泵的主要参数:设计流量 $Q=11.2\ m^3/s$,设计

收稿日期:2019-05-14 **修回日期**:2019-10-22 **网络出版时间**:2019-11-27
网络出版地址:http://kns.cnki.net/kcms/detail/13.1334.tv.20191127.1024.002.html
作者简介:吕蕊蕊(1994—),女,河南洛阳人,主要从事流体机械及工程方面研究。E-mail:773088653@qq.com
通信作者:郑源(1964—),男,山东日照人,教授,博士,主要从事流体机械及水利水电工程方面研究。E-mail:zhengyuan@hhu.edu.cn

扬程 $H=4.89$ m，转速 $n=250$ r/min，叶轮直径 $D=1640$ mm，叶片数 $Z_1=4$，导叶数 $Z_2=5$，轮毂直径 $d_h=600$ mm，三维模型见图 1。

图 1　轴流泵三维模型

1.2　湍流模型

数值模拟模拟方法有直接模拟和非直接模拟，由于直接模拟对计算资源需求较大，一般采用非直接模拟方法，非直接模拟中应用最广泛的是雷诺时均法，根据涡粘模型求解的湍动黏度有零方程、一方程、两方程模型，目前使用较多的为两方程模型，其中 k-ε 模型是应用最广泛、最可靠的湍流模型；而 SST 模型[25]实际上是 k-ε 与 k-w 的结合；PANS 模型是可以进行从直接模拟模型过渡到雷诺时均化模型的计算模型，这个过程由调整模型中的 f_k、f_ε 参数进行控制，$f_k=0$ 时表示直接对 N-S 方程求解即 DNS 模型，$f_k=1$ 时，说明控制方程复原到 RANS，f_ε 在高雷诺数时取值为 1 更为合适[26]，参考文献[27-28]取 $f_k=0.2$；由 Johansen[29] 等提出的滤波器湍流模型（filter-based model，FBM）是根据滤波器尺寸来计算，相比较标准 k-ε，该模型修正了湍流黏性系数 μ_t，计算公式为

$$\mu_t=\frac{C_\mu\rho k^2}{\varepsilon}F,\quad F=\min\left[1,C_3\frac{\lambda\varepsilon}{k^{3/2}}\right] \tag{1}$$

式中：F 为滤波函数；λ 为滤波尺寸，$C_3=1.0$，数值计算中当大于该滤波尺寸则直接求解，小于该尺寸使用 k-ε。

1.3　网格划分

使用 ANSYS ICEM 软件对轴流泵各个部件进行结构化网格划分，其中转轮和导叶采用周期性网格划分，网格见图 2。网格数量在一定程度上会影响计算结果，因此进行网格无关性验证，由于对水泵进行空化数值模拟，因此将叶片表面最低压力数值考虑在内，在设计流量下使用 FBM 模型对泵装置进行数值模拟，计算结果表 1。由表可以看出随着网格数不断增加效率、水头、叶片表面最低压力都趋于稳定，再增加网格数对计算结果并没有显著影响，后面三种方案计算结果基本一致，但方案 4 与方案 5 网格数较多导致计算时间较长，因此最终选取方案 3。

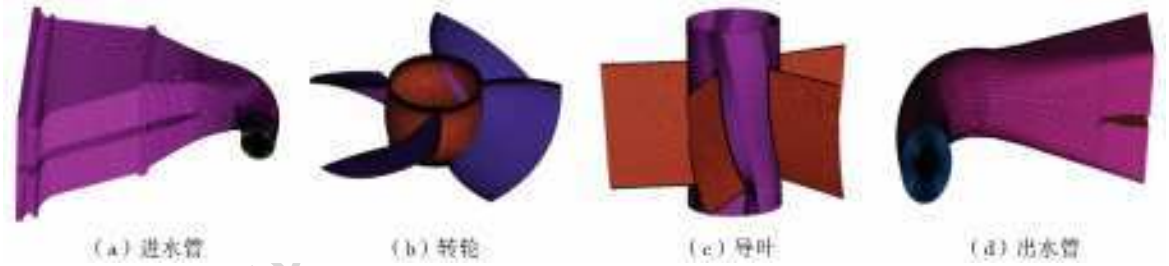

图 2　轴流泵结构化网格

表 1　网格无关性验证

方案	网格数/万个	效率/%	水头/m	叶片表面最低压力/Pa
1	300	76.32	4.89	-1.149×10^5
2	470	76.41	4.95	-1.147×10^5
3	600	76.48	5.01	-1.125×10^5
4	700	76.50	4.99	-1.124×10^5
5	800	76.51	4.98	-1.124×10^5

1.4　边界条件

流体介质选用 Water at 25 ℃、Water Vapour at 25 ℃，进口处气相体积分数为 0，液相体积分数为 1；进口处采用压力条件，出口处采用流量条件，转轮进出口的交界面设为 Frozen Rotor，收敛残差为 10^{-4}；水在 25 ℃饱和蒸汽压力设为 $P_v=3\,540$ Pa；为了提高计算速度，首先计算单相水，然后使用其结果作为初始条件，并添加空化模型以继续空化计算，且扬程与转轮内空泡体积分数趋于稳定时，可认为计算收敛。为使非定常计算收敛的更快，将空化定常结果作为非定常初始计算条件，时间步长设为0.000 365 76 s（转轮旋转 3 度），每步迭代次数为 5～15 次，动静交界面设置为 Transient Rotor Stator，总的计算时间为 30 T_n（由转速 $n=1\,367$ r/min 可得出 $T_n=0.043\,898\,16$ s），选取最后 5 个周期的数据进行分析。

2　试验装置及计算结果分析

2.1　试验装置

试验台示意图见图 3，试验台是立式封闭循环系统，有尾水箱、压水箱、不锈钢管路系统、电磁流量计、真空泵、供水泵、电动阀、手动蝶阀、扭矩仪等设备，试验综合误差≤0.4%。通过真空泵抽真空的方

式实现对水泵进口压力的控制,不断减小进口压力使水泵发生空化,空泡的分布情况通过拍摄获得。数值计算中的 NPSH、扬程 h 计算公式为

$$\mathrm{NPSH}=\frac{(P_a-P_v)}{\rho g} \tag{2}$$

$$h=\frac{(P_b-P_a)}{\rho g} \tag{3}$$

式中:P_a 为轴流泵进口总压,Pa;P_v 为 25 ℃饱和蒸汽压力3 540 Pa;$g=9.81$ N/m^2;P_b 为轴流泵出口压力,Pa;ρ 为水的密度1 000 kg/m^3。

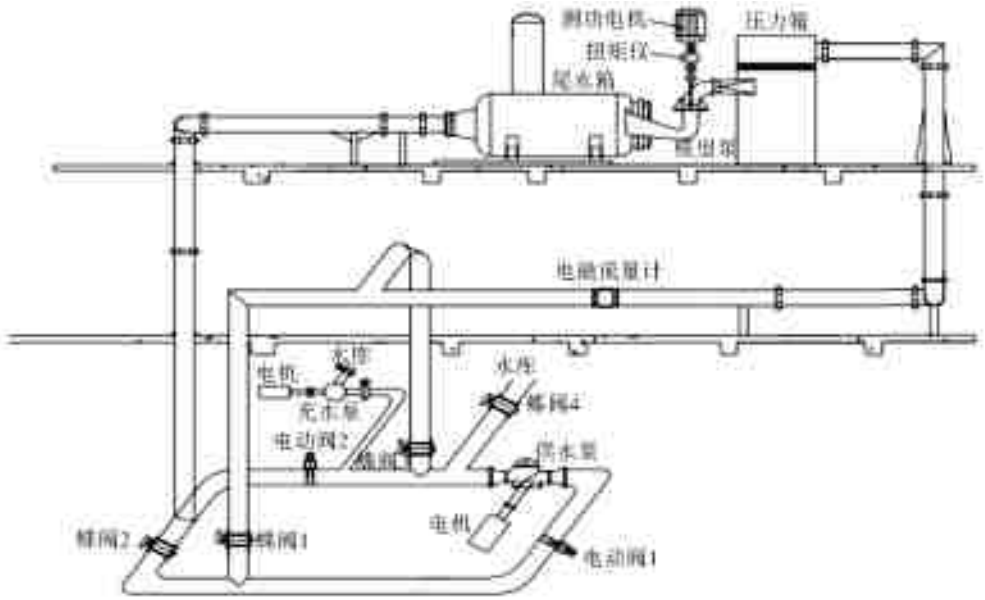

图 3　试验台装置示意图

2.2　外特性对比

取小流量工况下所有计算工况点的绝对误差的算术平均值为数值计算平均误差。由图 4 和表 2 可知,在设计流量下标准 k-ε 误差几乎为 0,后三种模型误差分别为 0.82%、2.45%、2.45%,设计工况下标准 k-ε 具有较好的适应性。大流量工况下随着流量增大,四种模型外特性计算误差不断增大,扬程计算误差分别为 2.65%～11.94%、2.43%～19.90%、3.76%～12.85%、2.43%～7.96%,所以 SST 模型在大流量工况下数模计算预测值的精度容易受工况变动影响,误差最大,而 FBM 预测数值相比较前三个模型与实验数值最为接近。PANS 模型在小流量工况下随着流量不断减少,其数模计算结果误差明显增大,扬程预测最大误差为 6.60%,平均扬程误差与扬程最大误差均明显大于其他三种模型,因此 PANS 模型在小流量工况下数模计算结果的精度容易受工况变动影响,误差最大;而 FBM 模型在小流量工况下平均扬程误差为 1.19%,平均效率误差为 5.31%,这两者数值明显低于其他三种湍流模型,因此 FBM 模型在轴流泵小流量工况流场计算中具有较高的精度,与实验数值几乎一致。

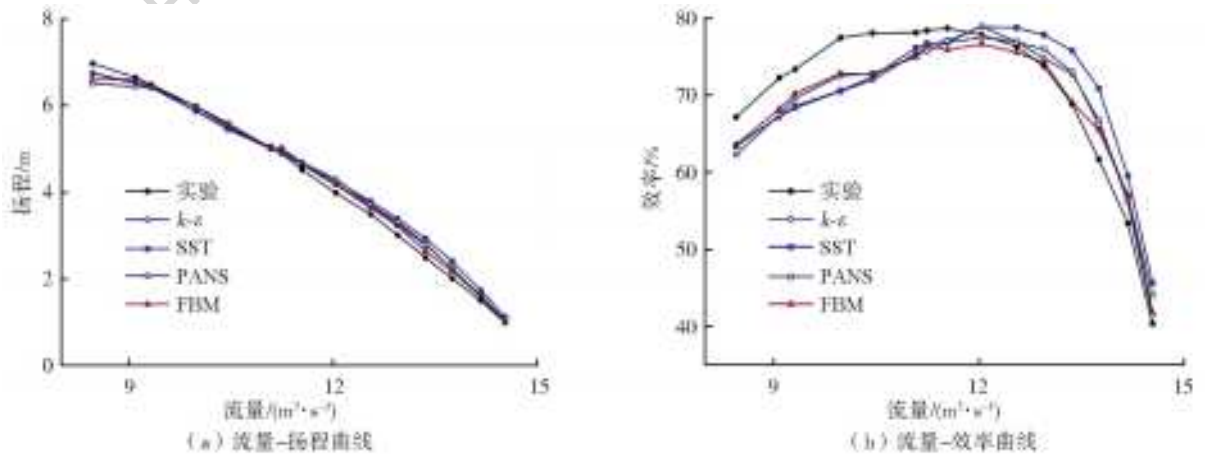

图 4　外特性预测与实验值对比

表 2　小流量工况下不同湍流模型数值计算平均误差

湍流模型	k-ε	SST	PANS	FBM
平均扬程误差/%	1.44	1.54	2.06	1.19
平均效率误差/%	6.58	6.27	5.98	5.31

2.3　实验与数值计算空化工况对比

由于要对两个具体空化工况点进行分析,将数值模拟 B(NPSH=5.25 m)、D(NPSH=3.72 m)工况与相应实验工况点进行对比见表 3,由表可知空化刚开始阶段效率误差为 0.94%,严重空化工况效率误差为 7.65%,严重空化工况下轴流泵内部流态极其复杂,空泡的出现具有较大的随机性,因此该工况数模结果与实验相差较大,但总体来说这两个工况点的误差在合理范围内。将 B、D 工况下转轮内的空泡图与实验图进行对比,空泡体积分数按照 0.1 以上显示见图 5,由图可知数值计算模拟的空泡分布图与实验拍摄到的照片大体一致,说明数值计算的两个空化工况能较为准确地模拟轴流泵内的空泡分布情况。

表 3　研究工况效率计算误差

工况点	效率/%	效率误差/%
数值模拟 B 工况	72.69	0.94
实验 B 工况	73.38	
数值模拟 D 工况	64.84	7.65
实验 D 工况	70.21	

图 5　实验与数值计算空泡分布

2.4　转轮内空泡体积对比分析

在转轮内定义某个径向截面,引入无量纲变量 span,其中 span=r/R,式中 r 为轮毂至该截面的半径长,R 为转轮室壁面距离轮毂的半径长,其中 span=0 时该截面为轮毂面,span=1 时该截面为叶轮室壁面。选取 span=0.1 的截面进行分析,将该截面与叶片相交的曲线记为 S,设 S 上某一点至进水边距离为 w_1,曲线 S 长为 q,引入变量 $w=w_1/q$,图 6 为不同空化工况下叶片截面空泡体积分数分布,横坐标代表沿叶片截面流线方向的位置,当 $w=0$ 时为叶片进口,$w=1$ 时为叶片出口,纵坐标为空泡体积分数。由图 6 可知,空泡大都出现在叶片吸力面并且向叶片出口发展,靠近轮毂处的叶片空泡主要集中在叶片中部到尾部,B 工况叶片截面 0.6 到 0.8 位置和 D 工况截面 0.9 到叶片出口位置处的 FBM 和 PANS 模型预测的空泡体积分数值明显高于前两个模型,其中 FBM 预测数值稍高于 PANS。

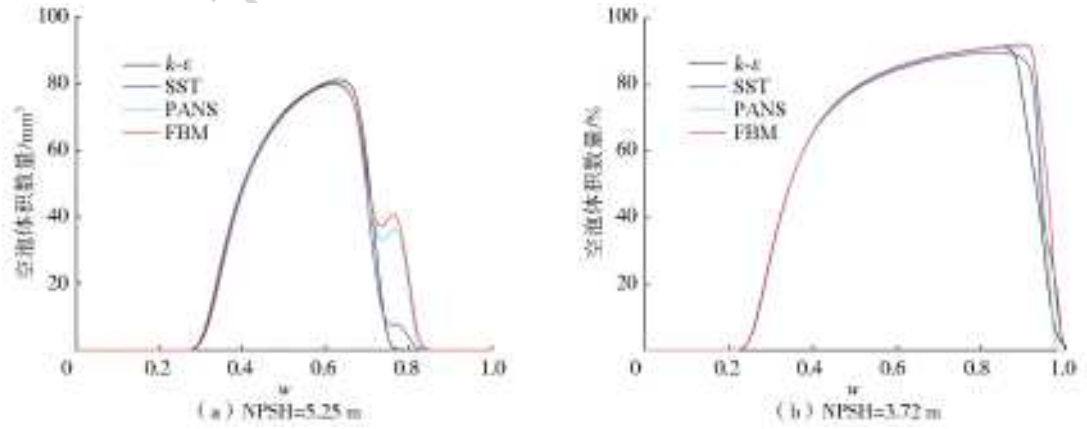

图 6　不同湍流模型叶片截面空泡体积分布

以 D 工况为例,在转轮内创建一个与转轮同高且上下底面同圆心的圆柱体,记轮毂半径为 r_1,叶轮半径为 r_2,该圆柱底面半径为 r,则横坐标 $t=(r-r_1)/(r_2-r_1)$,图 7 为随着数值 t 不断增大,该圆柱体内所含空泡体积数量的规律变化曲线。横坐标为 0 时,表示该圆柱体底面半径为轮毂半径,横坐标为 1 时,该圆柱体底面半径为叶轮半径。由图 7 可知,标准 k-ε 与 SST 模型预测的空泡体积数量曲

线比较贴合,PANS 与 FBM 模型计算所得的结果数值明显大于前两者,由于数值模拟往往在一定程度上低估了空化的发展,所以在预测空化性能这方面,标准 k-ε 与 SST 模型精度一般,PANS 精度高于前两者,结合图 6 和图 7 具体分析,FBM 模型在预测转轮叶片空泡体积数与含气率上精度最高。

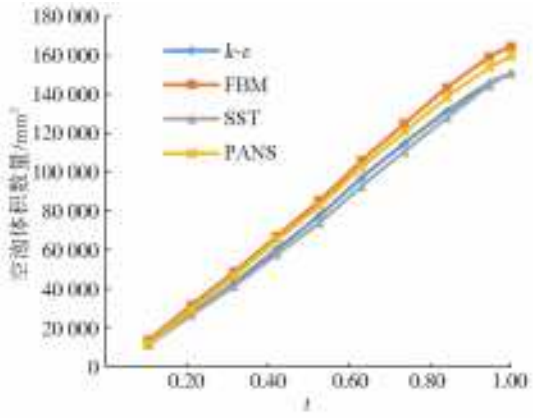

图 7　不同湍流模型转轮内空泡体积数量

3　空化工况下非定常分析

基于 FBM 湍流模型,选择设计流量下 B 工况进行非定常数值模拟,监测点设置见图 8。将数值计算得到的压力脉动进行傅里叶变换,由转速 n=1 367 r/min 可得出 f_n=22.78 Hz、T_n=0.043 898 16 s,为方便比较监测点压力脉动与机组转频之间的关系,取曲线横坐为 f/f_n。

3.1　导叶内部流场

在导叶内部选取监测点 dy1、dy2、dy3 所在的圆柱形截面进行分析,取时间间隔 0.1T_n,图 9 为叶轮旋转半个周期内随着时间变化的导叶内部流线图。由图可知在导叶片背面 1/2 处主要存在一种涡,记图中涡 A 出现的时间为 T_0(T_0=29T_n),叶片尾部的涡 B 向导叶出口扩散,T_0+0.2T_n 时刻涡 B 消失;T_0+0.3T_n 时刻在导叶片背面相同的位置出现涡C,T_0+0.3T_n到T_0+0.5T_n涡A随着主流的

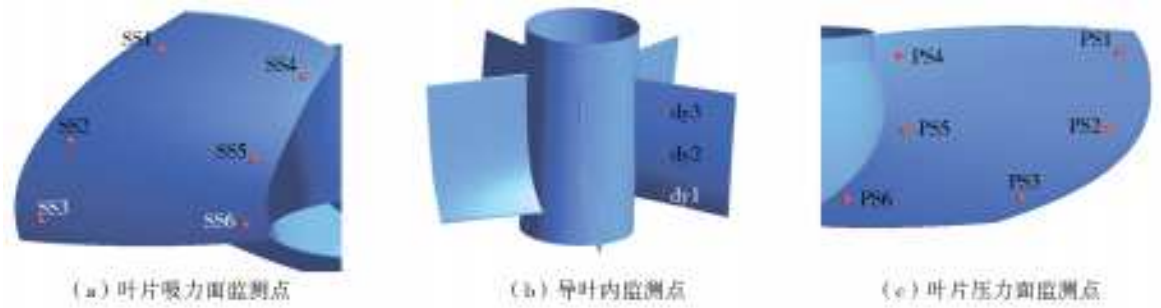

(a) 叶片吸力面监测点　(b) 导叶内监测点　(c) 叶片压力面监测点

图 8　压力监测点布置

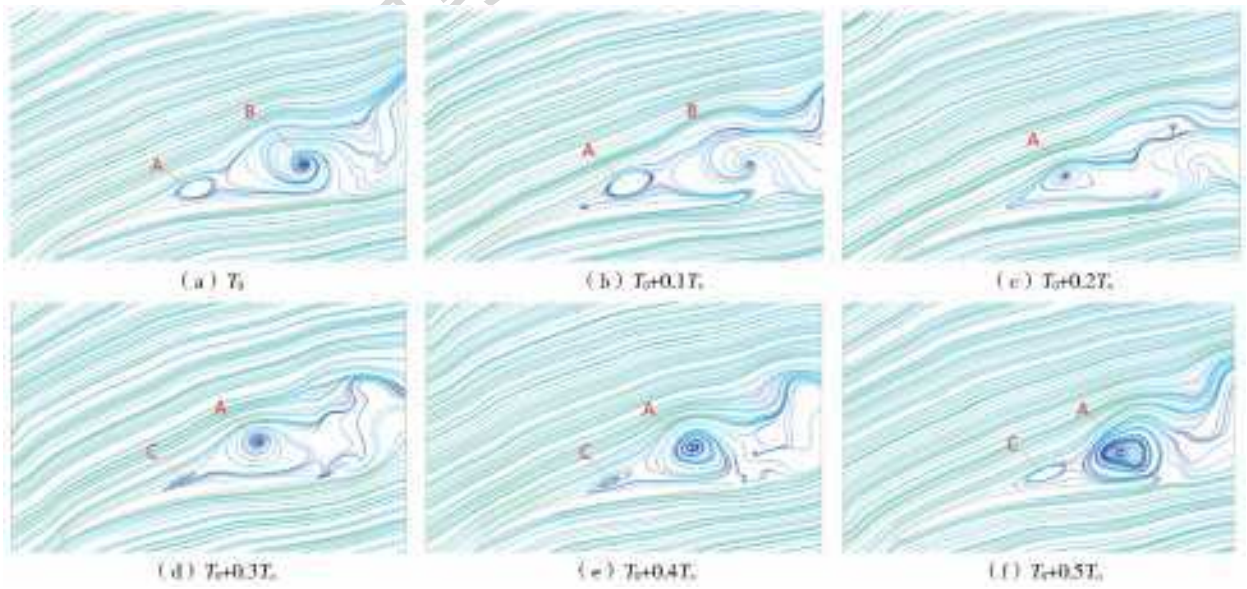

(a) T_0　(b) T_0+0.1T_n　(c) T_0+0.2T_n

(d) T_0+0.3T_n　(e) T_0+0.4T_n　(f) T_0+0.5T_n

图 9　导叶内部流线

方向不断增大,由于受计算条件限制,无法精确该涡产生的周期,参照 T_0 时刻涡 A 的形态,可知导叶片背面涡产生周期大约为 0.4T_n 到 0.5T_n,换算可得到该涡的频率大约为 2.0f_n 到 2.5f_n。

3.2　空化工况下压力脉动特性分析

由图 10 可知,机组转频 f_n 是影响叶片压力面

的压力脉动频率的主要因素,而叶轮出口靠近轮缘处的监测点 ss1 的压力脉动主要由导叶片通过频率 $5f_n$ 来确定,这是由于该监测点靠近转轮出口与导叶进口的动静交界面,因此导叶片的通过频率在此处的压力脉动起主导作用;由图 5 可得叶片背面产生了较大面积空泡,转轮室内大多为云状空泡,空泡运动到高压区会发生破裂,空泡的破裂常常带来很大的压力脉动,而空泡的溃灭速度很快,因此叶片吸力面上的监测点出现较大的分频幅值,由于空泡溃灭主要发生在叶片尾部,所以靠近叶轮出口的监测点 ss1 与 ss4 的压力脉动更复杂。叶轮进口处的 ss3 与 ss6 监测点的压力脉动主要由叶片通过频率 $4f_n$ 占据主导地位,其他监测点主频为机组转频。

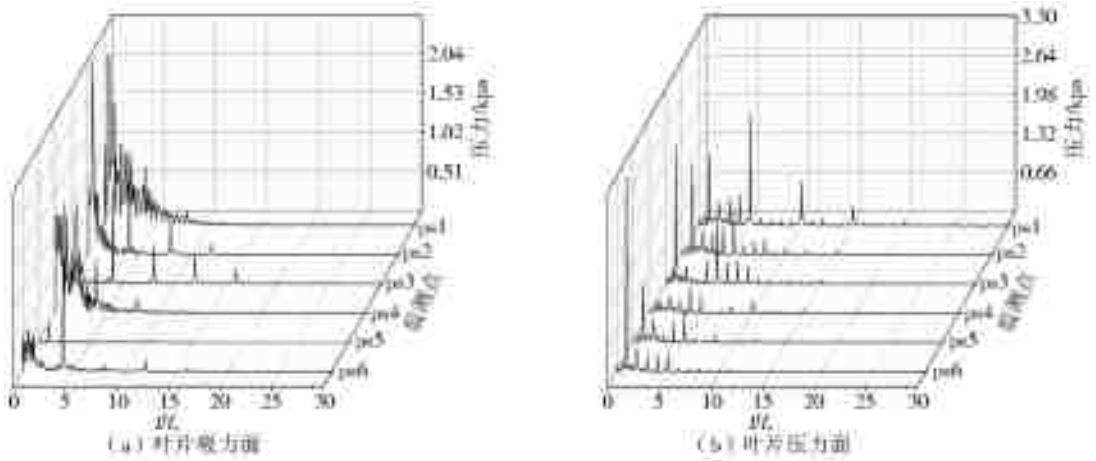

图 10　叶片监测点压力脉动频域

由于受到导叶片整流作用,流道内压力幅值减小,导叶片背面流态复杂出现较大区域旋涡,因此导叶流道中央 dy1、dy2 监测点的压力脉动具有一定的分频幅值,然而此处压力脉动的主要频率由叶片通过频率 $4f_n$ 决定;而靠近导叶出口处的 dy3 监测点,由于距离转轮较远,此处监测点受叶片旋转的影响较小,再加上导叶片背面 1/2 处周期性产生涡流,所以 dy3 处的压力脉动出现大量幅值较大的低频信息,由前述可知该涡主要频率大约为 $2.0f_n$ 到 $2.5f_n$,与图 11 中监测点 dy3 的几个低频压力脉动峰值对应的频率范围一致。

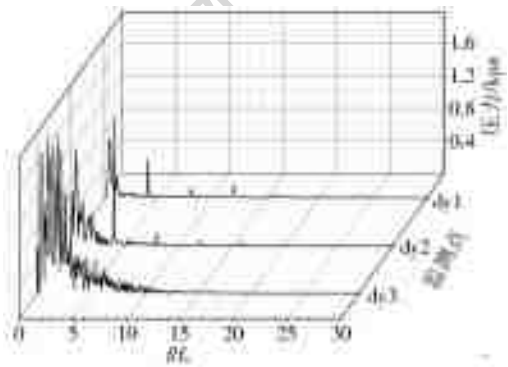

图 11　导叶内监测点压力脉动频域

4　结　论

(1)非设计工况下 FBM 模型预测外特性数值误差最小,小流量工况下平均扬程误差 1.19%,平均效率误差 5.31%,FBM 尤其在小流量工况流场计算中具有较高的精度;标准 k-ε 在设计工况下具有较好的适应性,大流量工况下 SST 模型和小流量工况下的 PANS 模型预测数值的误差波动较大,容易受工况变动影响,精度较差。

(2)FBM 模型在预测空泡体积数与含气量上的精度最高,与实验结果最接近;在预测轴流泵空化性能这方面,标准 k-ε 与 SST 模型精度一般,PANS 精度高于前两者。

(3)空化刚开始(NPSH=5.25 m)阶段,叶片上的压力脉动主要频率位于 f_n 及其倍频处;叶片工作面出口轮缘处的压力脉动主要由导叶的通过频率 $5f_n$ 确定,吸力面进口处压力脉动主要由叶片通过频率 $4f_n$ 占据主导地位,由于受到空泡溃灭的影响吸力面监测点出现较大的分频幅值;导叶片背面 1/2 处产生一主要频率大约 $2.0f_n$ 至 $2.5f_n$ 的涡,使得导叶出口靠近流道中央处的压力脉动出现大量的分频幅值。

参考文献:

[1]　刘超. 水泵及水泵站[M]. 北京:中国水利水电出版社,2009.

[2]　李忠. 轴流泵内部空化流动的研究[D]. 镇江:江苏大学,2011.

[3]　张德胜,吴苏青,施卫东,等. 轴流泵小流量工况条件下叶顶泄漏空化特性[J]. 农业工程学报,2013,29(22):

68-75.

[4] 张德胜,潘大志,施卫东,等. 轴流泵空化流及其诱导压力脉动的数值模拟[J]. 华中科技大学学报(自然科学版),2014,42(1):34-38.

[5] 侯敬生,袁建平,范猛,等. 轴流泵空化流动的非定常特性研究[J]. 中国农村水利水电,2017(11):174-178. DOI: CNKI:SUN:ZNSD. 0. 2017-11-037.

[6] 周大庆,刘敏,陈会向. 虹吸式出水流道轴流泵装置全流道空化特性[J]. 华中科技大学学报(自然科学版),2017, 45 (1): 128-132. DOI: 10. 13245/j. hust. 170124.

[7] 冯卫民,程千,郭志伟,等. 前置导叶可调式轴流泵低频压力脉动特性研究[J]. 农业机械学报,2015,46(10):62-67. DOI: 10. 6041/j. issn. 1000-1298. 2015. 10. 010.

[8] 王凡,钱忠东,郭志伟,等. 可调导叶式轴流泵压力脉动数值分析[J]. 农业机械学报,2017(3):124-128. DOI: 10. 6041/j. issn. 1000-1298. 2017. 03. 015.

[9] 施卫东,张光建,张德胜,等. 入口非均匀流对轴流泵性能和压力脉动的影响[J]. 排灌机械工程学报,2014,32(4):277-282.

[10] 宋希杰,刘超,罗灿. 轴流泵装置进水漩涡对压力脉动的影响[J]. 农业机械学报,2018,49(2):113-119,81. DOI: 10. 6041/j. issn. 1000-1298. 2018. 02. 015.

[11] 蒋文青,郑源,葛新峰. 某二维水翼空化数值模型对比研究[J]. 南水北调与水利科技,2017,15(3):204-208. DOI: 10. 13476/j. cnki. nsbdqk. 2017. 03. 033.

[12] 周颖,郑源,汪昊蓝,等. 不同空化条件下轴流泵反向发电压力脉动特性研究[J]. 南水北调与水利科技,2019,17(1):178-185. DOI: 10. 13476/j. cnki. nsbdqk. 2019. 0024.

[13] 施卫东,吴苏青,张德胜,等. 叶片数对高比转数轴流泵空化特性的影响[J]. 农业机械学报,2013,44(11):72-77.

[14] 陶迎. 轴流泵内部空化特性数值计算研究[D]. 武汉:华中科技大学,2015.

[15] MOSTAFA N H,MOHAMED A. Effect of blade angle on cavitation phenomenon in axial pump[J]. Journal of Applied Mechanical En ineering,2012,3(1):1-6.

[16] HOSONO K,KAJIE Y,SAITO S,et al. Study on cavitation influence for pump head in an axial flow pump [J]. Journal of Physics: Conference Series,2015(656): 012062. DOI: 10. 1088/1742-6596/656/1/012062.

[17] MOLOSHNYI O,SOTNYK M. Cavitation in centrifugal pump with rotating walls of axial inlet device [J]. IOP Conference Series Materials Science and Engineering,2017,233. DOI: 10. 1088/1757-899X/233/1/012007.

[18] WU S Q,SHI W D,ZHANG D S,et al. Influence of blade tip rounding on tip leakage vortex cavitation of axial flow pump[J]. IOP Conference Series: Materials Science and Engineering,2013,52(6):062011.

[19] 张德胜,施卫东,张华,等. 不同湍流模型在轴流泵性能预测中的应用[J]. 农业工程学报,2012,28(1):66-71.

[20] 石磊,张德胜,陈健,等. 基于 PANS 模型的轴流泵叶顶空化特性[J]. 排灌机械工程学报,2016,34(7):590-596. DOI: 10. 3969/j. issn. 1674-8530. 15. 0144.

[21] 张德胜,石磊,陈健,等. 基于 DCMFBM 模型的轴流泵叶顶区云状空化脱落预测[J]. 农业机械学报,2016,47(8):22-28. DOI: 10. 6041/j. issn. 1000-1298. 2016. 08. 004.

[22] 余志毅,时素果,黄彪,等. FBM 模型在栅中翼形空化流动计算中的应用[J]. 工程热物理学报,2010,31(5):777-780.

[23] 时素果,王国玉,余志毅,等. FBM 湍流模型在非定常通气超空化流动计算中的评价与应用[J]. 船舶力学,2012,16(10):1099-1106.

[24] FU Y,YUAN J,YUAN S,et al. Numerical and experimental analysis of flow phenomena in a centrifugal pump operating under low flow rates[J]. Journal of Fluids Engineering,2015,137(1):011102. DOI: 10. 1115/1. 4027142.

[25] 常书平,王永生. 基于 CFD 的混流泵空化特性研究[J]. 排灌机械工程学报,2012,30(2):171-175.

[26] DAVIDSON L. The PANS k-epsilon model in a zonal hybrid RANS-LES formulation [J]. International Journal of Heat & Fluid Flow,2014,46(4):112-126.

[27] 施卫东,张光建,张德胜. 基于 PANS 模型的水翼非定常空化特性研究[J]. 华中科技大学学报(自然科学版),2014,42(4):1-5.

[28] 黄彪,王国玉,权晓波,等. PANS 模型在空化湍流数值计算中的应用[J]. 应用力学学报,2011,28(4):339-343.

[29] JOHANSEN S T,WU J,WEI S. Filter-based unsteady RANS computations[J]. International Journal of Heat & Fluid Flow,2004,25(1):10-21.

·译文(Translation)·

DOI:10.13476/j.cnki.nsbdqk.2020.0017

CFD analysis of cavitation flow for axial-flow pump based on FBM model

LYU Ruirui, ZHENG Yuan, ZHANG Dehu, YU An

(College of Energy and Electrical Engineering Hohai University, Nanjing 211100, China)

Abstract: The working condition of the axial flow pump is changeable, and cavitation is easy to occur, which can seriously affect the hydraulic performance of a pump. To study the flow characteristics of the axial flow pump under cavitation condition, numerical simulations and pressure pulsation analysis of cavitation flow in full channel were carried out. The superiority of FBM model in predicting the external characteristics and cavitation performance of axial flow pump was verified by comparing the experimental data based on calculated results of different turbulence models. The results showed that the FBM model had least error in predicting external characteristics under non-design conditions, especially in the flow field under small flow conditions. The average lift error was 1.19%, and the average efficiency error was 5.31%, respectively. The accuracy of FBM in predicting cavitation volume and gas fractionwas higher than other three turbulence models, which was mostly close to the obtained experimental results. In the initial stage of NPSH=5.25 m cavitation, the main frequency of pressure pulsation on the blade was located at f_n, and its frequency was doubled, while large number of low-frequency amplitudes appeared at the pressure monitoring point on the suction surface of the blade due to the influence of cavitation collapse. The pressure pulsation at the outlet of the guide vane was influenced by the flow pattern on the back of the guide blade.

Key words: turbulence model; error; external characteristic; Cavitation performance; pressure fluctuation

Axial flow pump is widely used in irrigation, water supply, drainage, and other fields where large flow rate is needed because it has large flow rate and simple structure[1]. Cavitation in is an important factor affecting the stable operation of the pump, which produced strong water hammer and caused the corrosion of the flow passage parts of the unit[2]. Therefore, research on cavitation flow characteristics of the pump is of great significance. For example, ZHANG D S, HOU J S, et al[3-5]. carried out numerical simulation of full channel cavitation of axial flow pump by using SST k-w turbulence model; ZHOU D Q, FENG W M, WANG F, SHI W D SONG X J[6-10] analyzed the influence of guide vane angle, inlet uniform flow and inlet vortex on the pressure fluctuation characteristics of axial flow pump with SST k-w and RNG k-ε; JIANG W Q, et al.[11] simulated the process of cavitation flow around the hydrofoil and axial flow pump with RNG k-ε and SST k-w; ZHOU Y, et al.[12] analyzed the pressure pulsation characteristics of axial flow pump reverse generation under different cavitation conditions with k-ε; SHI W D, TAO Y, et al.[13-14] analyzed the influence of blade number, guide blade number and blade angle on cavitation performance of axial flow pump; MOSTAFA N H, HOSONO K, MOLOSHNYI O and WU S Q[15-18] mostly simulate the cavitation of wa-

Received: 2019-05-14 **Revised**: 2019-10-22 **Online publishing**: 2019-11-27
Online publishing address: http://kns.cnki.net/kcms/detail/13.1334.tv.20191127.1024.002.html
Author brief: LYU Ruirui(1994-), mainly engaged in research on fluid machinery and engineering. E-mail: 773088653@qq.com
Corresponding author: ZHENG Yuan(1964-), professor, mainly engaged in research on fluid machinery and Water conservancy and hydropower engineering. E-mail: zhengyuan@hhu.edu.cn

ter pump by k-ε.

The selection of turbulence model will affect the results of pump performance prediction to a certain extent[19]. In recent years, PANS and the modified model based on have been gradually applied to the numerical simulation of pump[20-21]. The results of YU Z Y, SHI S G, et al.[22-23] showed that the cavitation numerical simulation based on FBM can capture more flow details. However, few scholars applied FBM model for numerical simulations of axial flow pump cavitation. Therefore, in this paper, the FBM turbulence model was used to simulate the steady and unsteady cavitation of axial flow pump under designed flow, which may verify the accuracy of the numerical calculation of the model and analyze the pressure fluctuation characteristics in the runner and guide vane at the beginning of cavitation. The cavitation model of homogeneous flow based on Rayleigh Plesset equation is more applicable[24]. A number of scholars use this cavitation model in their studies, therefore, the homogeneous flow cavitation model based on ANSYS CFX is used to calculate the cavitation of axial flow pump.

1 Physical model and numerical calculation methods

1.1 Geometric model

In geometric model, main parameter of the pump, for example, design flow (Q=11.2 m^3/s), design lift (H=4.89 m), speed (n=250 r/min), impeller diameter (D=1 640 mm), number of blades (Z_1=4), number of guide vanes (Z_2=5), hub diameter (d_h=600 mm) were used. The 3D model diagram is shown in Fig. 1.

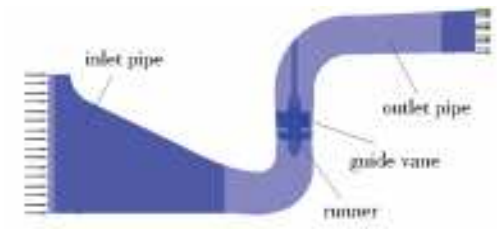

Fig. 1 Three-dimensional model of the axial flow pump

1.2 Turbulence model

There are direct and indirect simulations in numerical simulation. The indirect simulation method is generally used due to great demand for computing resources. The Reynolds time-averaged method is the most widely used in indirect simulation. According to the vortex viscosity model, there are zero, one and, two equation models. At present, two-equation models are widely used. For example, k-ε model is the most widely used and reliable turbulence model. SST model[25] is a combination of k-ε and k-w model. The PANS model is a computational model that can transition from a direct simulation model to a Reynolds time homogenization model. This process is controlled by adjusting the parameters of f_k and f_ε in the model, when f_k=0, it means to solve the N-S equation, while f_k=1, it means that the control equation is restored to RANS. It is more appropriate when f_ε=1[26]. In reference[27-28], f_k=0.2. The filter-based model (FBM) proposed by Johansen, et al.[29] and is calculated according to the size of the filter. Compared with the k-ε, the model(FBM) corrects the turbulent viscosity coefficient μ_t, and the calculation formula is as follows

$$\mu_t=\frac{C_\mu \rho k^2}{\varepsilon}F,\quad F=\min\left[1,C_3\frac{\lambda\varepsilon}{k^{3/2}}\right] \tag{1}$$

where F is the filter function, λ is the filter size, C_3=1.0. In the numerical calculation, if it is larger than the filter size, it will be solved directly, and if it is smaller than the size, k-ε will be used.

1.3 Grid division

The structural mesh of each part of the axial flow pump is divided by ANSYS ICEM, in which the runner and guide vane are divided by periodic mesh (Fig. 2). The number of grids can affect the calculation results to a certain extent, so the grid independence verification was carried out. Due to the cavitation numerical simulation of the water pump, the lowest pressure value on the blade surface was taken into account, and the FBM model was used to simulate the pump device under the design flow. The calculation results are shown in Tab. 1. It can be seen from the table that the efficiency, water head, and the minimum pressure on the blade surface tend to be stable with the increase of grid number, and the increase of grid-number has no significant impact on the calculation results . The calculation results of the latter three

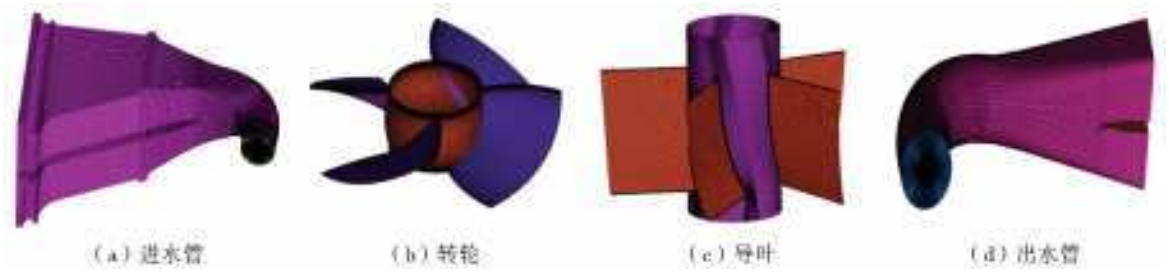

Fig. 2 Structured grid of axial flow pump

Tab. 1 Mesh independence verification

scheme	grid number/ million	efficiency/ %	lift/ m	minimum pressure on blade surface /Pa
1	3.0	76.32	4.89	-1.149×10^5
2	4.7	76.41	4.95	-1.147×10^5
3	6.0	76.48	5.01	-1.125×10^5
4	7.0	76.50	4.99	-1.124×10^5
5	8.0	76.51	4.98	-1.124×10^5

schemes were basically the same, but the calculation time was longer due to a large number of grids in scheme 4 and scheme 5. Thus scheme 3 was finally selected.

1.4 Boundary conditions

The fluid medium was water at 25 ℃, water vapour at 25%, the gas volume fraction at the inlet was 0, the volume fraction of the liquid phase was 1, the pressure condition was adopted at the inlet, the flow condition was assumed at the outlet, the interface between the inlet and the outlet of the runner was set to Frozen Roor, and the convergence residual was 1, respectively. The water pressure of the water was set to be 2 Pa. The saturated steam pressure of water at 25 ℃ was set as $P_v=3\,540$ Pa. In order to improve the calculation speed, firstly, single-phase water was calculated, and then the obtained result was used as the initial condition. Add cavitation model to continue the cavitation calculation, and when the lift and the volume fraction of the cavity in the runner tend to be stable, the calculation could be considered as convergence. In order to make the unsteady calculation convergence faster, the steady result of the cavitation was used as the unsteady initial calculation condition. The time step was set as 0.000 365 76 s (the runner rotates 3 degrees), the number of iterations per step is 5-15, the dynamic and static interface was set as the Transition Rotor Stator, and the total calculation time was 30T. The data of the last five periods were selected for analysis.

2 Test device and analysis of calculated results

2.1 Test device

The schematic diagram of the test-bed is shown in Fig. 3. The test-bed was a vertical closed circulation system. It had a tail water tank, a pressure water tank, a stainless steel pipe system, an electromagnetic flow meter, a vacuum pump, a water supply pump, an electric valve, a manual butterfly valve, a torque meter, and other types of equipment. The comprehensive test error was considered less than or equal to 0.4%. The control of the inlet pressure of the pump was realized by vacuum pumping, and the cavitation occured by reducing the inlet pressure continuously. The distribution of the cavitation was obtained by photographing. The formula of NPSH, lift h in numerical calculation can be find as follows

$$\mathrm{NPSH}=\frac{(P_a-P_v)}{\rho g} \tag{2}$$

$$h=\frac{(P_b-P_a)}{\rho g} \tag{3}$$

where P_a is the total pressure at the inlet of the axial flow pump (Pa); P_v is the 25 ℃ saturated steam pressure 3 540 Pa; $g=9.81$ N/m^2; P_b is the outlet pressure of the axial flow pump (Pa); ρ is the density of water 1 000 kg/m^3.

2.2 Comparison of external characteristics

The arithmetic mean value of the absolute error of all calculation points under the condition of small flow was taken as the average numerical error. It can be seen from Fig. 4 and Tab. 2 that the standard k-ε error was almost 0 under the design flow, and the errors of the last three models were 0.82%, 2.45%, and 2.45%, respectively.

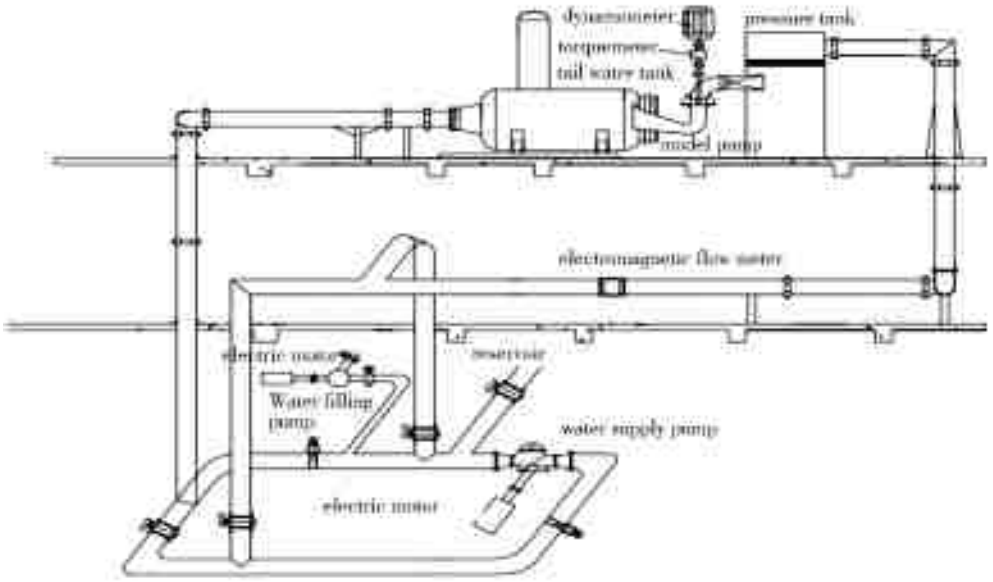

Fig. 3 The schematic diagram of the test-bed device

Under the design condition, k-ε had good adaptability. Under the condition of large flow, the error of the external characteristics of the four models was increasing with the increase of the flow, and the error of the lift was 2.65%～11.94%, 2.43%～19.90%, 3.76%～12.85%, 2.43%～7.96%, respectively. The accuracy of the model SST in the large flow condition was easy to be affected by the change of working conditions, which may produced large errort. The FBM prediction value was the closest to the experimental value. The error of numerical simulation results of PANS model increased with the decrease of flow rate. The maximum error of lift prediction was 6.60%. The average lift error and the maximum error of lift were significantly larger than the other three models. Therefore, the accuracy of numerical simulation results of PANS model was easily affected by the change of working conditions, while the error was large. The average lift error and average efficiency error of FBM model were 1.19% and 5.31% under the condition of small flow rate, which was obviously lower than those of the other three turbulence models. Therefore, the FBM model had high accuracy in the calculation of flow field of axial flow pump under small flow condition, which was almost consistent with the experimental value.

2.3 Comparison between experimental and numerical cavitation conditions

Two specific cavitation condition points were analyzed, and the numerical simulation B (NPSH=5.25 m) and D (NPSH=3.72 m) conditions were compared with the corresponding experimental condition points, as shown in Tab 3. It can be seen from the Table 3 that the efficiency error in the initial stage of cavitation was 0.94%, and the efficiency error in the

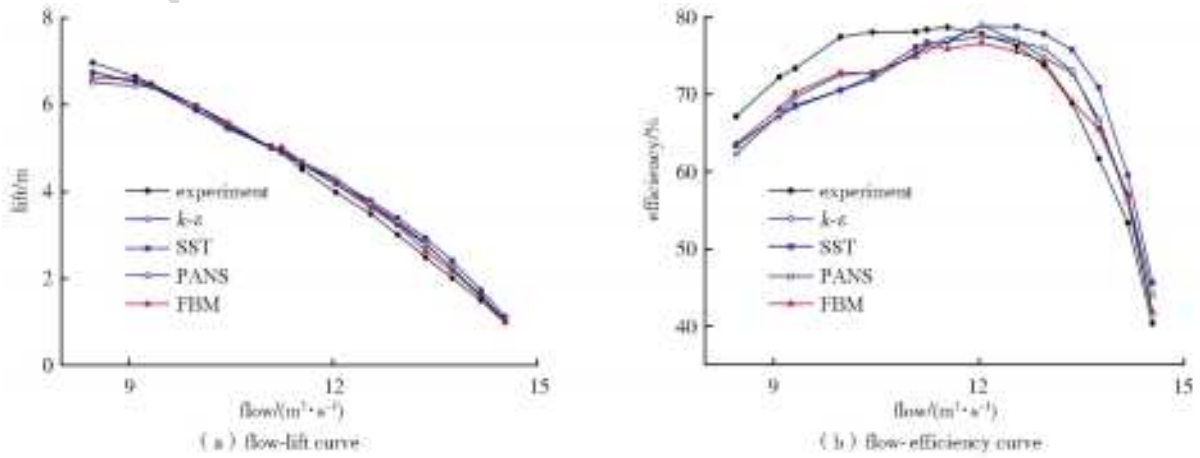

Fig. 4 Comparison diagram of external characteristics prediction and experimental values

severe cavitation condition was 7.65%, respectively. Under the severe cavitation condition, the internal flow state of axial flow pump was extremely complex, and the occurrence of cavitation had great randomness. Therefore, the results of numerical simulation were quite different from the experimental results, but the errors of these two operating points were in a reasonable range. Compare the cavitation diagram in the runner under B and D conditions with the experimental diagram, and the volume fraction of the cavitation is shown in Fig. 5. According to the Fig. 5 above 0.1. It can be seen from the figure that the cavitationdistribution diagram simulated by the numerical calculation was generally consistent with the photos taken by the experiment, which showed that the two cavitation conditions calculated by the numerical calculation could accurately simulate the cavitation distribution in the axial flow pump.

Tab. 2 Average error in numerical simulation of different turbulence models under small flow condition

Turbulence model	k-ε	SST	PANS	FBM
Average lift error /%	1.44	1.54	2.06	1.19
Average efficiency error /%	6.58	6.27	5.98	5.31

Tab. 3 Calculation error of study working condition efficiency

Operating point	Efficiency/%	Efficiency error/%
Numerical simulation condition B	72.69	0.94
Experimental condition B	73.38	
Numerical simulation condition D	64.84	7.65
Experimental condition D	70.21	

Fig. 5 Experimental and numerical calculation of cavitation distribution diagram

2.4 Comparison of the cavitation volume in the runner

A radial section was defined in the runner. In the dimensionless variable span (span = r/R), r was the radius from the hub to the section, R was the radius from the runner chamber wall to the hub. When span = 0, the section was the hub surface, while span = 1, the section was the impeller chamber wall surface. For analysis, span = 0.1 was selected. Fig. 6 showed the distribution of cavitation volume fraction of blade section under different cavitation conditions. The curve of the cross-section and the blade was recorded as S, the distance between a point on the note S and the inlet edge of the blade was t, the length q of the curve S was q, The variable $w = w_1/q$ was introduced Figure 6 showed the distribution of cavitation volume fraction of blade section under different cavitation conditions. The abscissa represented the position along the streamline direction of blade section. When the value of abscissa was 0, it was the blade inlet, while abscissa at 1, it was the blade outlet , and the vertical coordinate

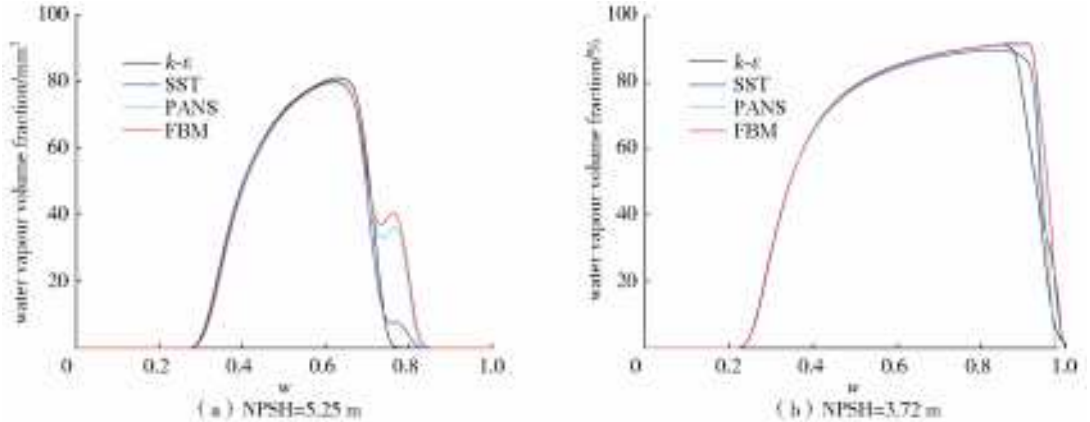

Fig. 6 The distribution of cavitation volume on blade sections of different turbulence models

was the cavitation volume fraction. It can be seen from the figure that most of the cavitation occurred on the suction surface of the blade and developed toward the outlet of the blade. The cavitation near the hub was mainly concentrated in the middle to the tail of the blade. The predicted value of FBM and PANS model for blade section were 0.6 to 0.8 in B condition and blade section 0.9 to blade outlet in D condition was significantly higher than that of the first two models, and the predicted value of FBM was slightly higher than PANS.

A cylinder with the same height and the center of the upper and lower bottom surfaces of the runner was created. The radius of the hub was r_1, the radius of the impeller was r_2, and the radius of the cylinder bottom wasa r, then the abscissa $t=(r-r_1)/(r_2-r_1)$. Fig. 7 showed the regular change curve of the number of cavitation in the cylinder with the increase of numerical value t. When the value of abscissa was 0, it means that the radius of the bottom of the cylinder was the radius of the hub; while the value of abscissa at 1, the radius of the bottom of the cylinder was the radius of the impeller. It can be seen from Figure 7 that the cavitation volume curve predicted by k-ε and SST model was relatively close, and the calculated results of PANS and FBM model were significantly larger than those of the first two turbulence models. Because numerical simulation often underestimate the development of cavitation to a certain extent, the accuracy of k-ε and SST model was general in predicting cavitation performance, and the accuracy of PANS model was higher than that of the first two models. Combined with the specific analysis of Fig. 6 and Fig. 7, FBM model had the highest accuracy in predicting the cavitation volume number and gas fraction of runner blades.

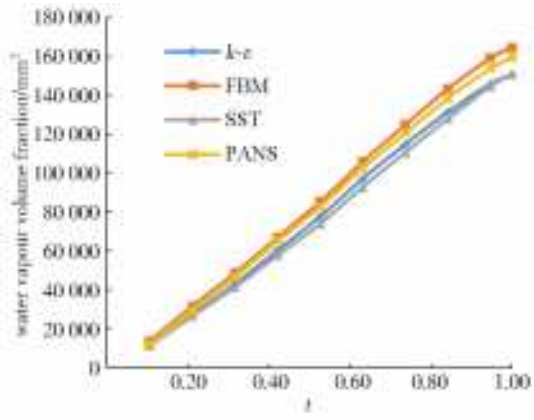

Fig. 7 Volume fraction of cavitation in runner with different turbulence models

3 Unsteady analysis under cavitation condition

The unsteady numerical simulation was carried out under condition B under the design flow based on the FBM turbulence model, and the setting of monitoring points is shown in Fig. 8. The pressure pulsation obtained by numerical calculation was transformed by Fourier transform, $f_n=22.78$Hz、$T_n=0.043\ 898\ 16$ s which could be obtained from the rotating speed $n=1\ 367$ r/min. To facilitate the comparison of the relationship between the pressure pulsation at the monitoring point and rotational frequency, the abscissawas taken as f/f_n.

3.1 Flow field in guide vane

The cylindrical section of the monitoring points dy1, dy2, dy3 were selected for analysis in the guide vane. Fig. 9 showed the streamline diagram inside the guide vane with interval of fetch time $0.1T_n$ during the half cycle of impeller rotation. It can be seen from the diagram that there was mainly a kind of vortex at 1/2 on the back of the guide vane. The time of the vortex A in the figure was T_0 ($T_0=29T_n$). The vortex B at the tail of the blade diffused at the exit of the guide blade, while vortex B disappeared at $T_0+0.2T_n$. Vortex

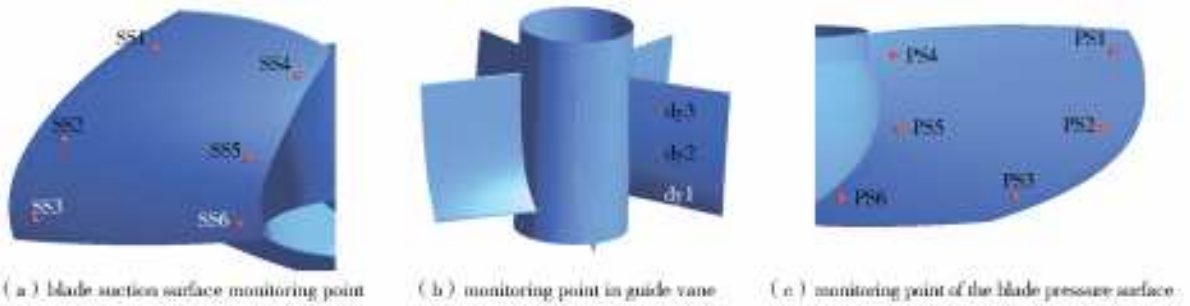

(a) blade suction surface monitoring point (b) monitoring point in guide vane (c) monitoring point of the blade pressure surface

Fig. 8 Layout of pressure monitoring points

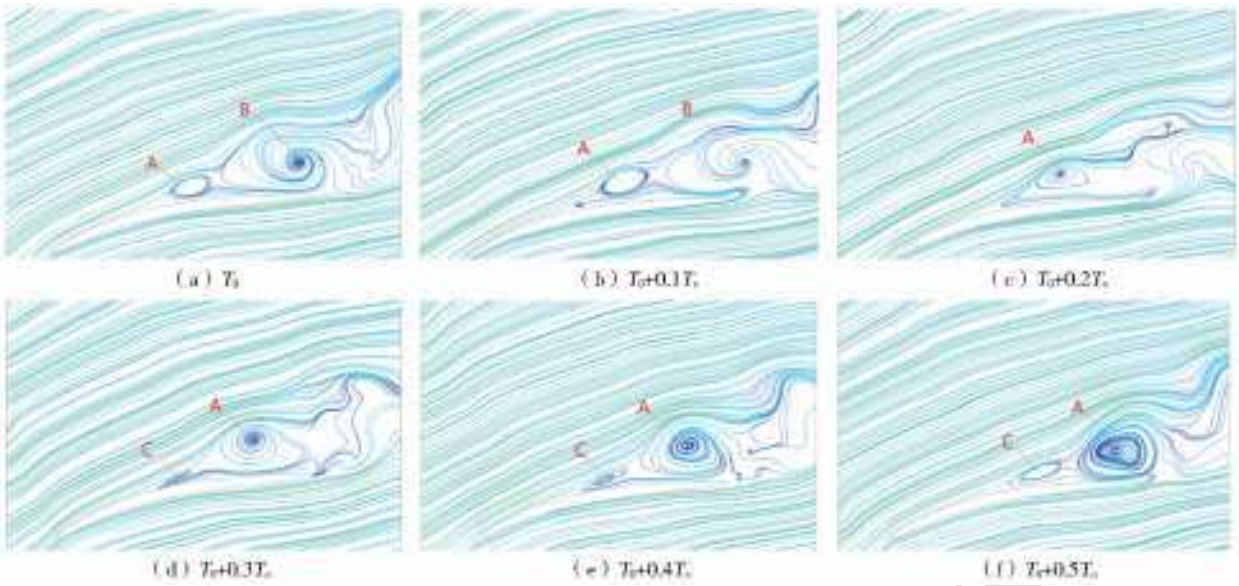

Fig. 9 Streamline diagram inside guide vane

C appears at $T_0+0.3T_n$ at the same position on the back of guide vane, and vortex A from $T_0+0.3T_n$ to $T_0+0.5T_n$ increased with the mainstream direction. Due to the limitation of calculation conditions, it is impossible to produce the vortex period accurately. Referring to the shape of vortex at the time of T_0, it can be seen that the generation period of the vortex on the back of the guide vane was about $0.4T_n$ to $0.5T_n$, and the frequency of the vortex could be about $2.0f_n$ to $2.5f_n$.

3.2 Analysis of pressure fluctuation characteristics under cavitation condition

It can be seen from Fig. 10 that the rotational frequency was the main factor that affect the pressure fluctuation frequency of the blade's pressure surface, the pressure fluctuation of the monitoring point ss1 at the impeller outlet near the flange was mainly determined by passing frequency of guide blade ($5f_n$), which was due to monitoring point that was close to the dynamic and static interface between the impeller outlet and the guide vane inlet. The pressure pulsation of the guide vane played a leading role here. It can be seen from Fig. 5 that a large area of cavitation occurred at the back of the blade. There was mostly cloud cavitation in the runner. When the cavitation moved to the high-pressure area, it cloud break. The breaking of the cavitation often brings great pressure pulsation, and the collapse speed of the cavitation was very fast, so the monitoring points on the suction surface of the blade have a large amplitude of frequency division. Because the cavitation collapse mainly occurred at the tail of the blade, the pressure fluctuation of ss1 and ss4 near the impeller outlet was more complex. The pressure pulsation of ss3 and ss6 at the impeller inlet was mainly dominated by the blade passing frequency ($4f_n$),

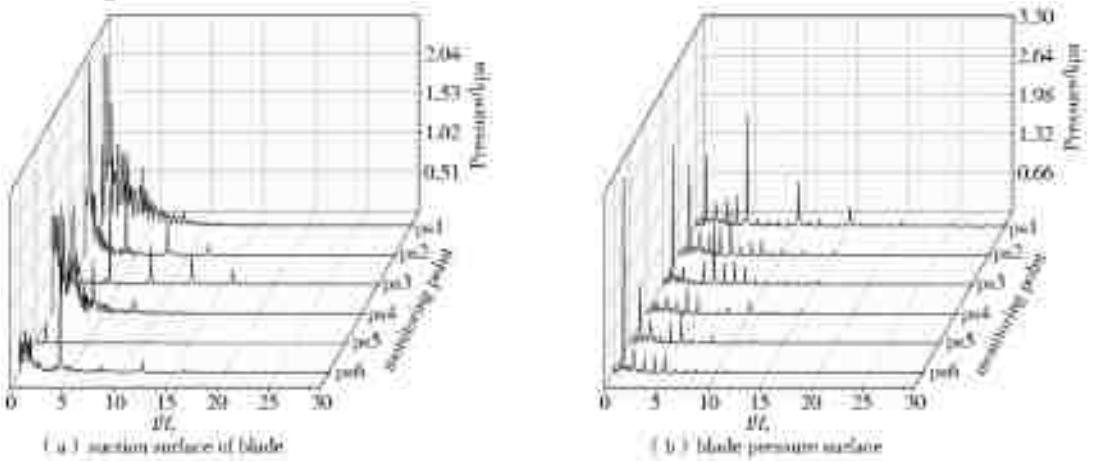

(a) suction surface of blade (b) blade pressure surface

Fig. 10 Frequency domain diagram of pressure fluctuation at the blade monitoring point

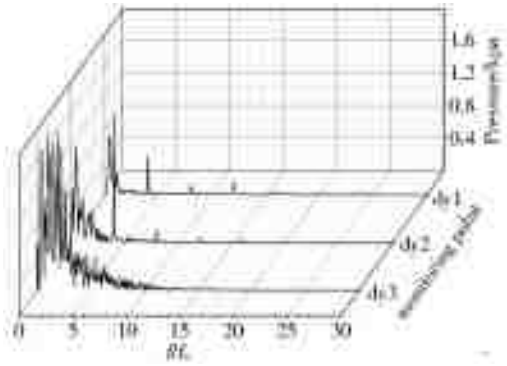

Fig. 11 Frequency domain diagram of pressure pulsation at monitoring points in guide vane

and the main frequency of other monitoring points was the rotational frequency.

Due to the effect of the guide vane rectification, the pressure amplitude in the flow channel decreased. The flow pattern on the back of the guide blade was complex, and a large area vortex appeared. Therefore, the pressure pulsation at the monitoring points of dy1 and dy2 in the center of the guide vane channel had a certain amplitude or frequency division. However, the main frequency of pressure pulsation was determined by the blade passing frequency. However, the monitoring point dy3 near the outlet of guide vane was far away from the runner, and the pressure fluctuation of this monitoring point was less affected by the rotation of the blade. In addition, 1/2 of the back of the guide vane periodically generated eddy current. Therefore, a large amount of low-frequency information with a large amplitude appeared in the pressure pulsation at dy3. It can be seen from the above that the main frequency of the vortex was about $2.0f_n$ *to* $2.5f_n$, which was consistent with the frequency range corresponding to several low-frequency pressure pulsation peaks at monitoring point dy3 in the Fig. 11.

4 Conclusions

(1) The prediction error of the FBM model under non-design condition was the smallest, the average lift error under small flow condition was 1.19%, and the average efficiency error was 5.31%, respectively. FBM had high accuracy especially in the calculation of flow field under small flow condition. The standard k-ε had good adaptability under design condition, and the prediction error of SST model and PANS model was easy to be affected by the change of working conditions under large flow conditions and had low accuracy.

(2) The accuracy of the FBM model in predicting cavitation volume and gas fraction was the highest, which was closest to the experimental results. In predicting cavitation performance of axial-flow pump, the accuracy of k-ε and SST model was general, and the accuracy of PANS was higher than the former two models.

(3) At the beginning of cavitation (NPSH = 5.25 m), the main frequency of pressure pulsation on the blade was located at the f_n and the pressure fluctuation at the outlet edge of the blade working face was mainly determined by passing frequency of guide blade ($5f_n$), and the pressure pulsation at the inlet of the suction surface was mainly dominated by the blade passing frequency ($4f_n$), because the impact of cavitation collapse, the monitoring point of the suction surface had a large amplitude of frequency division. A vortex with frequency of $2.0f_n$ to $2.5f_n$ was generated at 1/2 of the back of the guide vane, and a large amplitude of frequency division appeared at the outlet of the guide vane that was near the center of the flow channel.

References:

[1] LIU C. Pumps and pump stations[M]. Beijing: China Water Power Press, 2009. (in Chinese)

[2] LI Z. Study on cavitation flow in Axial flow pump[D]. Zhenjiang: Jiangsu University, 2011. (in Chinese)

[3] ZHANG D S, WU S Q, SHI W D, et al. Characteristics of tip leakage vortex cavitation in axial flow pump at small flow rate condition[J]. Transactions of the Chinese Society of Agricultural Engineering, 2013, 29 (22): 68-75. (in Chinese)

[4] ZHANG D S, PAN D Z, SHI W D, et al. Numerical simulation of cavitation flow in axial flow pump and induced pressure fluctuation[J]. Journal of Huazhong University of Science and Technology (Natural Science Edition), 2014, 42(1): 34-38. (in Chinese)

[5] HOU J S, YUAN J P, FAN M, et al. Research on the unsteady characteristics of cavitating flow in the axial flow pump [J]. China Rural Water and Hydropower, 2017(11): 174-178. (in Chinese) DOI: CNKI: SUN: ZNSD. 0. 2017-11-037.

[6] ZHOU D Q, LIU M, CHEN H X. Siphon outlet conduit on full passage cavitation characteristics of axial-flow pumping unit[J]. Journal of Huazhong University of Science

and Technology (Natural Science Edition), 2017, 45(1): 128-132. (in Chinese) DOI:10.13245/j.hust.170124.

[7] FENG W M, CHENG Q, GUO Z W, et al. Characteristics of low frequency pressure fluctuation in axial flow pump with variable inlet guide vane[J]. Transactions of the Chinese Society for Agricultural Machinery, 2015, 46(10): 62-67. (in Chinese) DOI: 10.6041/j.issn.1000-1298.2015.10.010.

[8] WANG F, QIAN Z D, GUO Z W, et al. Pressure oscillations prediction of axial flow pump with adjustable guide vanes[J]. Transactions of the Chinese Society for Agricultural Machinery, 2017(3): 124-128. (in Chinese) DOI: 10.6041/j.issn.1000-1298.2017.03.015.

[9] SHI W D, ZHANG G J, ZHANG D S, et al. Effect of Inlet non-uniform flow on performance and pressure fluctuation of axial flow pump[J]. Journal of Drainage and Irrigation Machinery Engineering, 2014, 32(4): 277-282. (in Chinese)

[10] SONG X J, LIU C, LUO C. Influence of inlet vortex on pressure pulsation in axial-flow pump unit[J]. Transactions of the Chinese Society for Agricultural Machinery, 2018, 49(2): 113-119, 81. (in Chinese) DOI:10.6041/j.issn.1000-1298.2018.02.015.

[11] JIANG W Q, ZHENG Y, GE X F. Comparative numerical study of cavitation on a two-dimensional hydrofoil[J]. South-to-North Water Transfers and Water Science & Technology, 2017, 15(3): 204-208. (in Chinese) DOI:10.13476/j.cnki.nsbdqk.2017.03.033.

[12] ZHOU Y, ZHENG Y, WANG H L, et al. Study on fluctuation characteristics of axial-flow pump in reverse power generation under different cavitation conditions[J]. South-to-North Water Transfers and Water Science & Technology, 2019, 17(1): 178-185. (in Chinese) DOI: 10.13476/j.cnki.nsbdqk.2019.0024.

[13] SHI W D, WU S Q, ZHANG D S, et al. Effects of number of blades on cavitation of high specific speed axial flow pump[J]. Transactions of the Chinese Society for Agricultural Machinery, 2013, 44(11): 72-77. (in Chinese)

[14] TAO Y. Numerical research of cavitation flow in axial flow pump[D]. Wuhan: Huazhong University of Science and Technology, 2015. (in Chinese)

[15] MOSTAFA N H, MOHAMED A. Effect of blade angle on cavitation phenomenon in axial pump[J]. Journal of Applied Mechanical En ineering, 2012, 3(1): 1-6.

[16] HOSONO K, KAJIE Y, SAITO S, et al. Study on cavitation influence for pump head in an axial flow pump[J]. Journal of Physics: Conference Series, 2015(656): 012062. DOI:10.1088/1742-6596/656/1/012062.

[17] MOLOSHNYI O, SOTNYK M. Cavitation in centrifugal pump with rotating walls of axial inlet device [J]. IOP Conference Series Materials Science and Engineering, 2017, 233. DOI: 10.1088/1757-899X/233/1/012007.

[18] WU S Q, SHI W D, ZHANG D S, et al. Influence of blade tip rounding on tip leakage vortex cavitation of axial flow pump[J]. IOP Conference Series: Materials Science and Engineering, 2013, 52(6): 062011.

[19] ZHENG D S, SHI W D, ZHANG H, et al. Application of different turbulence models for predicting performance of axial flow pump[J]. Transactions of the Chinese Society of Agricultural Engineering, 2012, 28(1): 66-71. (in Chinese)

[20] SHI L, ZHANG D S, CHEN J, et al. characteristics of tip cavitation in an axial-flow pump based on PANS model[J]. Journal of Drainage and Irrigation Machinery Engineering, 2016, 34(7): 590-596. (in Chinese) DOI:10.3969/j.issn.1674-8530.15.0144.

[21] ZHANG D S, SHI L, CHEN J, et al. Prediction of cloud cavitation shedding in tip region of axial flow pump based on DCMFBM turbulence model[J]. Transactions of the Chinese Society for Agricultural Machinery, 2016, 47(8): 22-28. (in Chinese) DOI: 10.6041/j.issn.1000-1298.2016.08.004.

[22] YU Z Y, SHI S G, HUANG B, et al. Application of FBM model in calculation of airfoil cavitation flow in gate[J]. Journal of Engineering Thermophysics, 2010, 31(5): 777-780. (in Chinese)

[23] SHI S G, WANG G Y, YU Z Y, et al. Evaluation of the filter-based turbulence model(FBM) for computation of unsteady ventilated-supercavitating flows[J]. CSSRC Reports, 2012, 16(10): 1099-1106. (in Chinese)

[24] FU Y, YUAN J, YUAN S, et al. Numerical and experimental analysis of flow phenomena in a centrifugal pump operating under low flow rates[J]. Journal of Fluids Engineering, 2015, 137(1): 011102. DOI: 10.1115/1.4027142.

[25] CHANG S P, WANG Y S. Study on cavitation characteristics of mixed-flow pump based on CFD[J]. Journal of Drainage and Irrigation Machinery Engineering, 2012, 30(2): 171-175. (in Chinese)

[26] DAVIDSON L. The PANS k-epsilon model in a zonal hybrid RANS-LES formulation[J]. International Journal of Heat & Fluid Flow, 2014, 46(4): 112-126.

[27] SHI W D, ZHANG G J, ZHANG D S. Investigation of unsteady cavitation around hydrofoil based on PANS model[J]. Journal of Huazhong University of Science and Technology (Natural Science Edition), 2014, 42(4): 1-5. (in Chinese)

[28] HUANG B, WANG G Y, QUAN X B, et al. Application of PANS model in numerical calculation of cavitation turbulence[J]. Chinese Journal of Applied Mechanics, 2011, 28(4): 339-343. (in Chinese)

[29] JOHANSEN S T, WU J, WEI S. Filter-based unsteady RANS computations[J]. International Journal of Heat & Fluid Flow, 2004, 25(1): 10-21.